



Contents lists available at ScienceDirect

Journal of Asian Earth Sciences

journal homepage: www.elsevier.com/locate/jseas

Evolution of Ataúro Island: Temporal constraints on subduction processes beneath the Wetar zone, Banda Arc

Kim S. Ely ^{a,*}, Mike Sandiford ^a, Margaret L. Hawke ^a, David Phillips ^a, Mark Quigley ^b,
Joao Edmundo dos Reis ^c

^a School of Earth Sciences, University of Melbourne, Victoria 3010, Australia

^b Department of Geological Sciences, University of Canterbury, Christchurch 8140, New Zealand

^c State Secretariat for Natural Resources, Edifício Fomento, Rua Dom Aleixo Corte Real, Mandarim, Dili, Timor-Leste

ARTICLE INFO

Article history:

Received 23 July 2010

Received in revised form 26 December 2010

Accepted 19 January 2011

Available online xxxx

Keywords:

Timor-Leste

Volcanology

Slab rupture

Uplift

Arc-continent collision

ABSTRACT

Ataúro is a key to understanding the late stage volcanic and subduction history of the Banda Arc to the north of Timor. A volcanic history of bi-modal subaqueous volcanism has been established and new whole rock and trace element geochemical data show two compositional groups, basaltic andesite and dacite-rhyolite. $^{40}\text{Ar}/^{39}\text{Ar}$ geochronology of hornblende from rhyo-dacitic lavas confirms that volcanism continued until 3.3 Ma. Following the cessation of volcanism, coral reef marine terraces have been uplifted to elevations of 700 m above sea level. Continuity of the terraces at constant elevations around the island reflects regional-scale uplift most likely linked to sublithospheric processes such as slab detachment. Local scale landscape features of the eastern parts of Ataúro are strongly controlled by normal faults. The continuation of arc-related volcanism on Ataúro until at least 3.3 Ma suggests that subduction of Australian lithosphere continued until near this time. This data is consistent with findings from the earthquake record where the extent of the Wetar seismic gap to a depth of 350 km suggests slab breakoff, as a result of collision, commenced at ~4 Ma, leading to subsequent regional uplift recorded in elevated terraces on Ataúro and neighbouring islands.

© 2011 Elsevier Ltd. All rights reserved.

1. Introduction

Arc-continent collision plays a significant role in the tectonic development of the Earth, and is a major process resulting in crustal growth. Areas of arc-continent collision are also amongst the most seismically active regions on Earth, thus understanding the evolution of these systems has important implications across a broad range of geoscience disciplines. Young arc-continent collision zones provide the best opportunity to investigate the early stages of collision, evidence of which is likely to be obscured in older orogens (Hall and Wilson, 2000). One of the world's youngest arc-continent collisions, between the northern margin of the Australian continent and the Banda Arc, provides an exceptional opportunity to study the initial evolution of an orogenic system.

The volcanic island of Ataúro lies in the centre of the Banda Arc collision zone, a 400 km long segment extending from Alor to Wetar (Fig. 1). Key features of this zone, known as the Wetar zone (Sandiford, 2008), are the cessation of volcanism around 3 Ma (Abbott and Chamalaun, 1981) and subsequent uplift of the arc (Chappell and Veeh, 1978; Hantoro et al., 1994). GPS studies have demonstrated the almost complete accretion of the Wetar zone

and the island of Timor to the Australian continent (Bock et al., 2003; Genrich et al., 1996; Nugroho et al., 2009). Following the onset of collision, the focus of deformation in the region has transferred from north-dipping subduction to south-dipping thrusts situated north of the volcanic chain (McCaffrey, 1988). These characteristics have been related to a putative rupture of the subducting Australian Plate slab (e.g. Sandiford, 2008), however, the details of the proposed mechanisms are not clear. This is in part because the geology and timing of events in the Wetar zone are only poorly understood. To address this, an investigation of the geology of Ataúro encompassing aspects of the volcanic and limestone stratigraphy, uplift, deformation and timing relationships has been undertaken. Prior to this study Ataúro had been the subject of only limited geochemical and geochronological studies (Abbott and Chamalaun, 1981; Whitford et al., 1977). In this study, the distribution and relationships of the various volcanic lithologies that comprise the island, and the nature and extent of the overlying reef limestone terraces, are established by geological mapping.

The key objective of this study is to provide new constraints on the termination of volcanism in the Wetar zone and subsequent deformation. New whole rock and trace element geochemical data are used to demonstrate the similarities between Ataúro and neighbouring islands, thus verifying a common volcanic evolution. New $^{40}\text{Ar}/^{39}\text{Ar}$ geochronology is presented, which confirms that

* Corresponding author. Tel.: +61 3 868 49771.

E-mail address: kimberlite1@gmail.com (K.S. Ely).

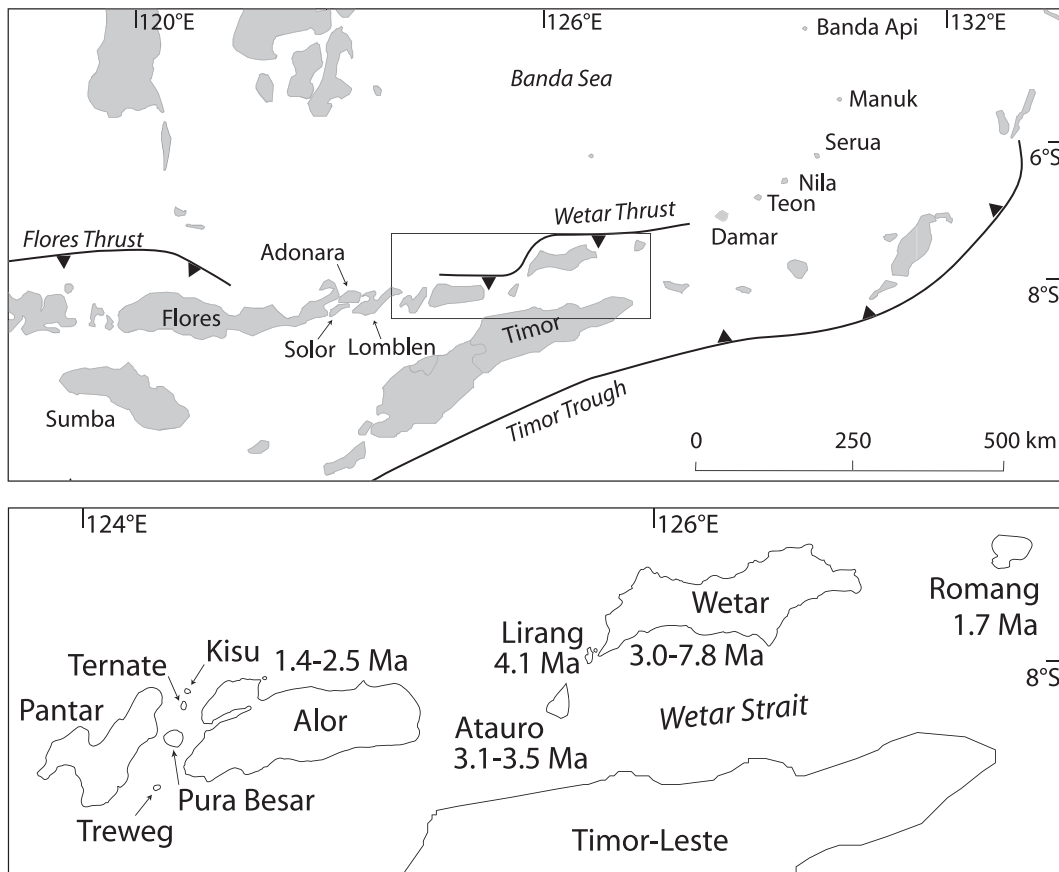


Fig. 1. Location of Ataúro in the Banda Arc. Inset map shows detail of inactive section of the volcanic arc, including a summary of the ages of volcanic rocks. Geochronological data from Abbott and Chamalaun (1981), Elburg et al. (2005), Hilton et al. (1992), Honthaas et al. (1998) and Scotney et al. (2005).

volcanism continued until around 3 Ma, and provides a basis on which to establish minimum uplift rates. Remnant volcanic landforms are only evident in the southwest of Ataúro; the dominant landform controls are uplifted marine terraces, normal faulting and significant erosion. One particular aim of this paper is to discriminate between the contribution of sublithospheric and crustal processes to the uplift and faulting observed on Ataúro. The geological history established as part of this study shows that uplift across all of Ataúro has been of significant magnitude and has been accompanied by little or no tilting, thus suggesting the influence of regional-scale processes as the dominant control of uplift, locally modified by east–west extension.

2. Geology of Ataúro

Ataúro is an elongate island, 22 km long and 10 km wide across the southwest end, with a maximum elevation of 1000 m. The island is formed by a volcanic edifice mantled by a spectacular succession of uplifted limestone coral reefs. The geological relationships are illustrated on Fig. 2. The dominant landforms are strongly controlled by the geology, comprising flat to sloping limestone terraces, steep hills and deeply dissected valleys cut into the volcanic substrate. Evidence of remnant volcanic landforms only occurs in the southwest, where the 800 m high, conical, twin peaked Mt. Berau and Mt. Tutonairana represent eruptive centres (Fig. 3a). A prominent escarpment, termed here the Vila Escarpment, can be traced north from the southeast corner of the island, where it forms coastal cliffs up to 300 m high (Fig. 3b–c). This escarpment divides the island into two geomorphically distinct regions. Coral reef terraces are only well preserved west of the

escarpment. East of the escarpment the stratigraphy is dissected by a series of arcuate north to northeast trending normal faults and terrace surfaces are now tilted to the west. With the exception of a single freshwater spring source north of Berau, the island is devoid of surface water during the dry season from May to October. The coastline typically comprises long beaches with fringing reefs, with some areas of mangrove mudflats on the east coast and cliffs dominating the southern coastline (Fig. 3d).

The volcanic stratigraphy of Ataúro comprises a varied succession of subaqueous lavas and volcaniclastic deposits, locally intruded by dykes and sills. Brecciated lavas of dacitic to rhyolitic composition dominate the sequence. Existing geochronology suggests the last eruptions were around 3 Ma (Abbott and Chamalaun, 1981) and hydrothermal activity continues today in the form of intertidal zone hot springs. Zones of hydrothermal alteration within the volcanic sequence have also been identified, and are associated with hot springs in several locations. The only significant prior contribution to the volcanic history of Ataúro is the K-Ar dating of samples from two sites on the south coast, and one site on the east coast (Abbott and Chamalaun, 1981). In addition, Whitford et al. (1977) reported major element and strontium isotope geochemistry of four samples from the south coast locations.

2.1. Pliocene volcanic units

The volcanic succession of Ataúro comprises two major lithologies, dacite and basaltic andesite. Dacite is the most common lithology, and occurs as lavas, breccias and volcaniclastic sequences.

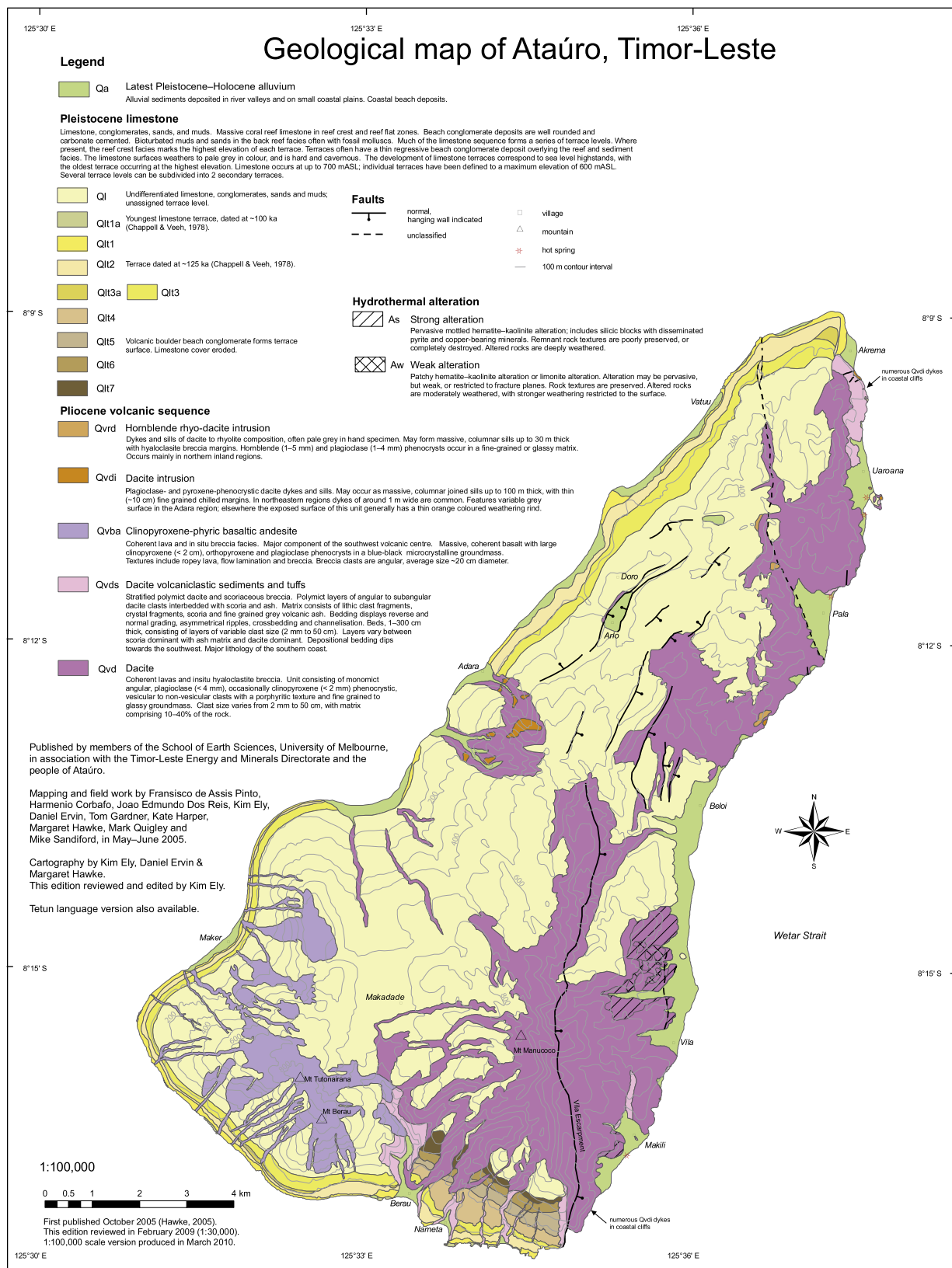


Fig. 2. Geological map of Ataúro, Timor-Leste.

2.1.1. Dacite

Porphyritic dacite is widespread across the northern and eastern parts of Ataúro, where it most commonly occurs as an *in situ*

hyaloclastite breccia of angular to sub-angular clasts up to 50 cm within a matrix comprising 10–40% of the rock (Fig. 4a). Coherent lava flows are also observed. Plagioclase phenocrysts are common,

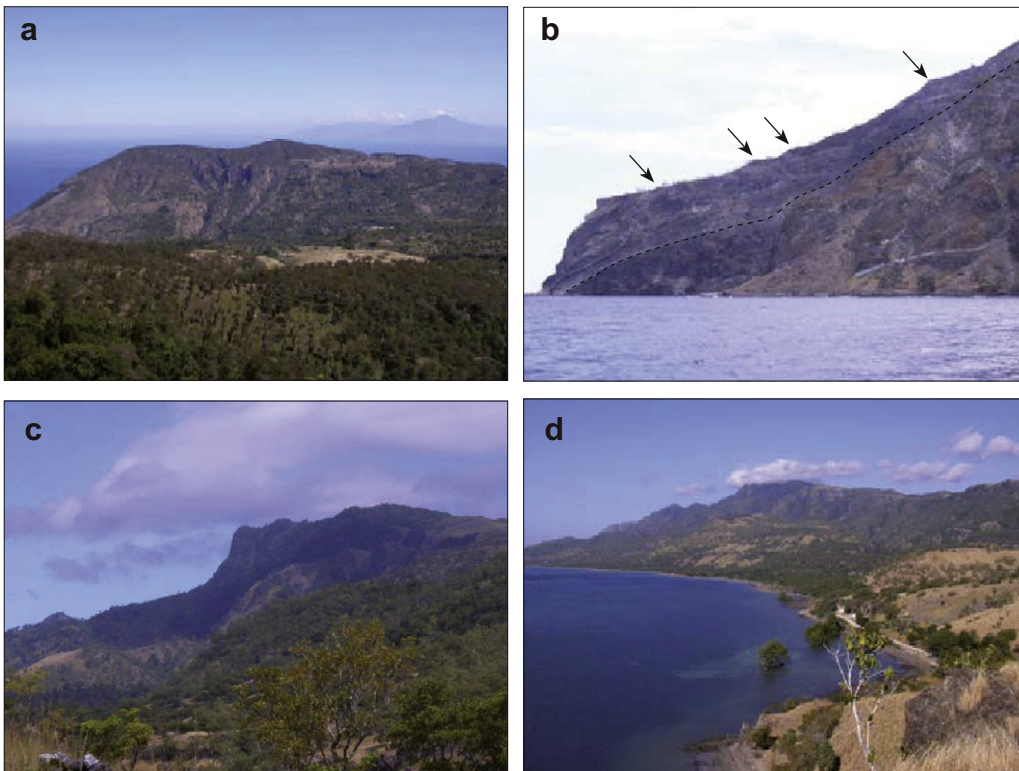


Fig. 3. Landforms of Ataúro. (a) Remnant volcanic cone landform of the southwest volcanic centre. The island of Alor can be seen on the horizon. (b) Cliffs of the Vila Escarpment, along the southeastern coastline, showing terraces in cross section. Arrows indicate outer reef margins; dashed line indicates contact between dacite lava flows and overlying volcanoclastic deposits. (c) Looking south along the Vila Escarpment, which forms the steep eastern flank of Mt. Manucoco, the highest point of Ataúro. (d) Looking south along the eastern coastline from north of Beloi. Sandy beaches are indispersed with low rocky headlands.

and a compositional range is represented by various proportions of pyroxene and hornblende phenocrysts. Mineral textures suggest that the dacite may be of cumulate origin, as clots of plagioclase and pyroxene or hornblende are common (Fig. 5a–b). Less commonly, all three minerals occur together. Plagioclase phenocrysts with sieve-texture rims occur in some samples (Fig. 6a–b). The groundmass is fine-grained to glassy, and glassy variants often exhibit perlitic textures (Fig. 5c). The groundmass is often brecciated, or, less commonly, flow textures are evident (Fig. 5d–f).

2.1.2. Resedimented dacite

Volcanoclastic sedimentary deposits are the dominant unit of southeastern Ataúro, where thick southwest-dipping sequences of tuffaceous sediments outcrop along the Vila Escarpment. The southwest dip direction is also recorded in other occurrences of this unit, including those on the northeast coast, implying deposition from a source located to the northeast of the island. Subangular dacite clasts up to 50 cm are typically supported in a matrix consisting of finer lithic fragments, broken crystals, scoria and volcanic ash (Fig. 5g–h). Bedding thickness is highly variable, from less than one centimetre to several metres, and may feature normal or reverse grading. Channels, ripples, crossbedding and flame structures are observed throughout the sequence (Fig. 4b–e).

2.1.3. Clinopyroxene-phyric basaltic andesite

A distinctive basaltic andesite unit featuring large clinopyroxene phenocrysts (1 cm), along with smaller plagioclase and olivine phenocrysts in a fine-grained, crystalline groundmass is observed only in the southwest of the island (Fig. 6c–d). It occurs as massive south to southwest dipping lava flows, and less commonly as angular, *in situ* breccia. Pillow lavas and lava tubes are exposed on the south coast (Fig. 4f). The down slope orientation of the lava tubes,

combined with flow directions interpreted from elongate vesicles, supports the presence of a single volcanic centre in the vicinity of the high ridge formed by Mt. Berau and Mt. Tutonairana, now at 800 m above sea level.

2.1.4. Other volcanic rock variants

Numerous other volcanic rock types, mostly dykes and sills of limited outcrop extent, occur within the volcanic succession. In the northeast, clinopyroxene-phyric dacite dykes up to 1 m wide with narrow chilled margins are exposed on coastal platforms and cliffs (Fig. 4g). Larger sills occur in the southeast, where massive plagioclase- and clinopyroxene-phenocrystic dacite sills up to 100 m thick exhibit columnar jointing and narrow chilled margins (Fig. 4h). Hornblende-bearing rhyo-dacite dykes and sills occur as pale grey, fine-grained rocks that intrude dacite, mainly in northern inland regions (Fig. 6e–h). Individual dykes can be traced for several hundred metres. These hornblende-bearing rhyo-dacite dykes were sampled for the $^{40}\text{Ar}/^{39}\text{Ar}$ geochronology presented in this paper.

2.2. Pliocene? – Pleistocene sedimentary units

Much of the volcanic edifice is mantled by limestone that forms spectacular terraces around the island. The lower level terraces are continuous around the south, west and north coasts of the island, but not east of the Vila Escarpment. Limestone also occurs over much of the inland parts of the island, up to elevations of 700 mASL. Across much of the inland region individual terrace levels are not easily distinguished because of extreme karstification (Fig. 7a). Areas where this is the case are classified on the geological map as undifferentiated limestone. Based on sections exposed near Berau, on the south coast, Chappell and Veeh (1978) showed each major terrace to comprise an individual reef structure

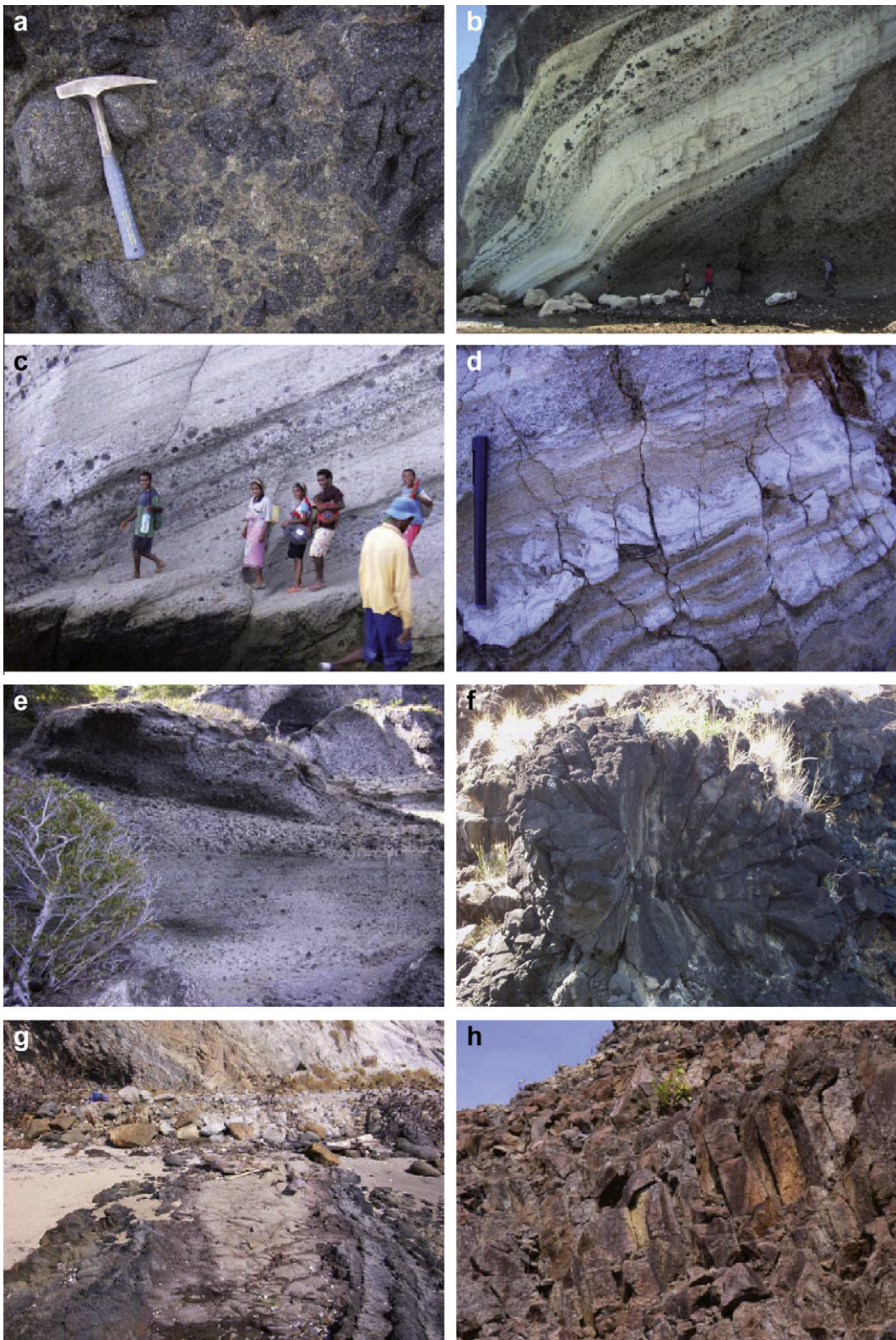


Fig. 4. Volcanic units of Ataúro. (a) Hyaloclastite texture in dacite (east coast, north of Pala). Hammer 33 cm long. (b) Volcaniclastic deposit (8.30371°S, 125.58382°E). (c) South-dipping volcaniclastic sediments (8.30636°S, 125.58346°E). (d) Flame structures in fine volcaniclastic sediments (east coast, north of Pala). (e) Stratified volcaniclastic deposits with channel cut and fill. Cliff face approximately 5 m high (8.30707°S, 125.58067°E). (f) Radial jointing in a lava tube on south coast (1.5 m wide, 8.27599°S, 125.50680°E). (g) Clinopyroxene-phyric dacite dyke (1.3 m wide) with chilled margins (8.14303°S, 125.64044°E). (h) Dacite lava flow with columnar jointing. Distinct columns in centre of photograph approximately 2 m high (8.29521°S, 125.58682°E).

analogous to the modern fringing reef. Subsidiary terrace levels formed by erosional benches are also present at lower terrace levels. Thus the uplifted terrace sequence preserves a record of

constructional (i.e. reef building) and erosional phases of development. Chappell and Veeh (1978) dated the youngest terrace (1a, ~20 mASL) at ~100,000 years and terrace 2 (~60 mASL) at

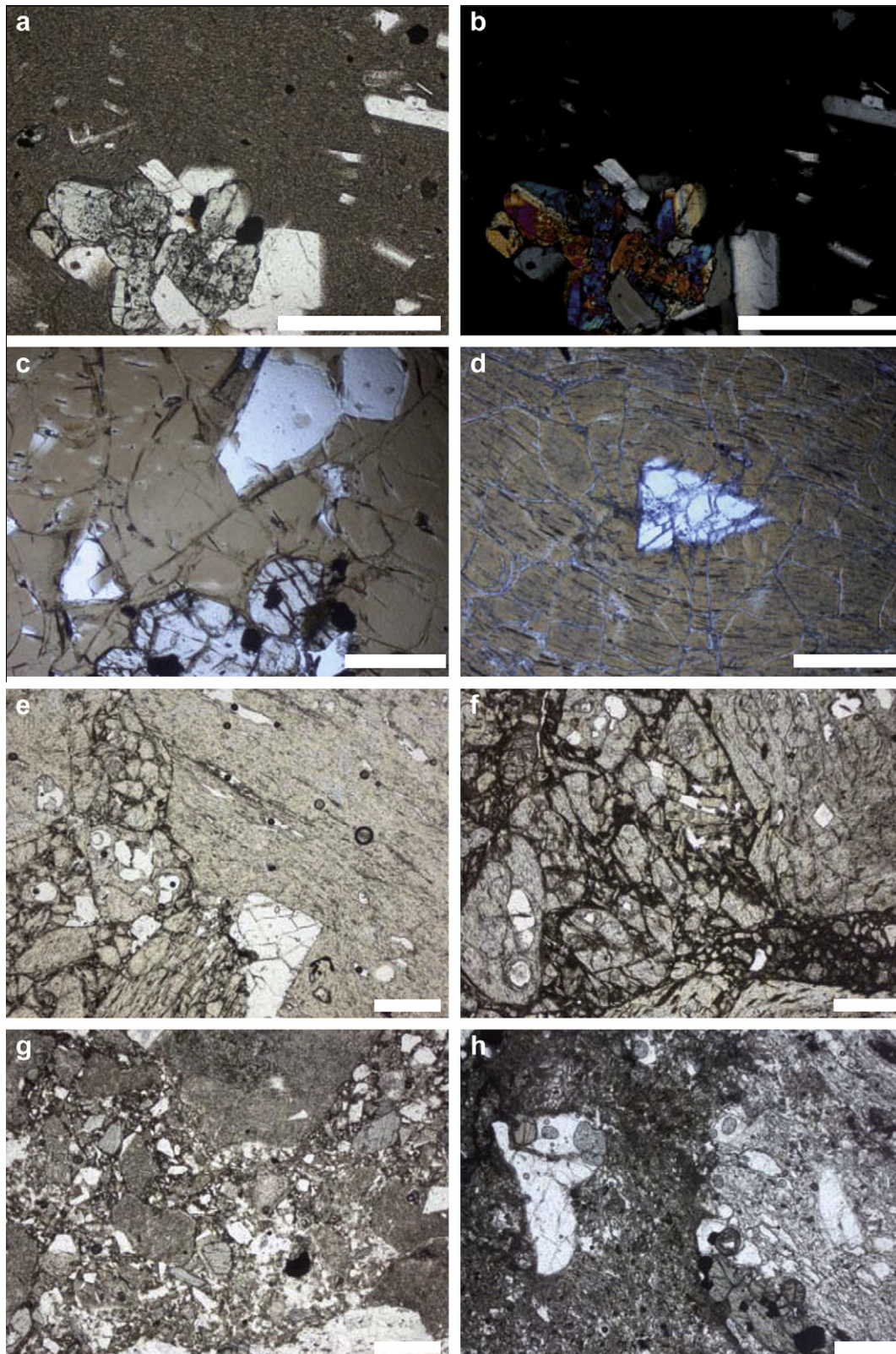


Fig. 5. Photomicrographs of representative volcanic textures. (a and b) Dacite (A05_007). (c) Perlitic fracture in glass (A05_119). (d) Flow banding in dacite (A05_085). (e and f) Brecciated dacite from east coast (A05_117a). (g) Volcaniclastic dacite, northern Ataúro (A05_016). (h) Volcaniclastic dacite, southern Ataúro (A05_019). Scale bar in all images is 0.5 mm long.

~125,000 years. Giant clams (*Tridacna* species) and corals preserved in growth position within the reef framework are observed at all terrace elevations (Fig. 7b–c). The reef complexes are often

overlain, and occasionally interbedded, with lag deposits comprising rounded volcanic cobbles similar to present-day beach cobbles common on the southern coast.

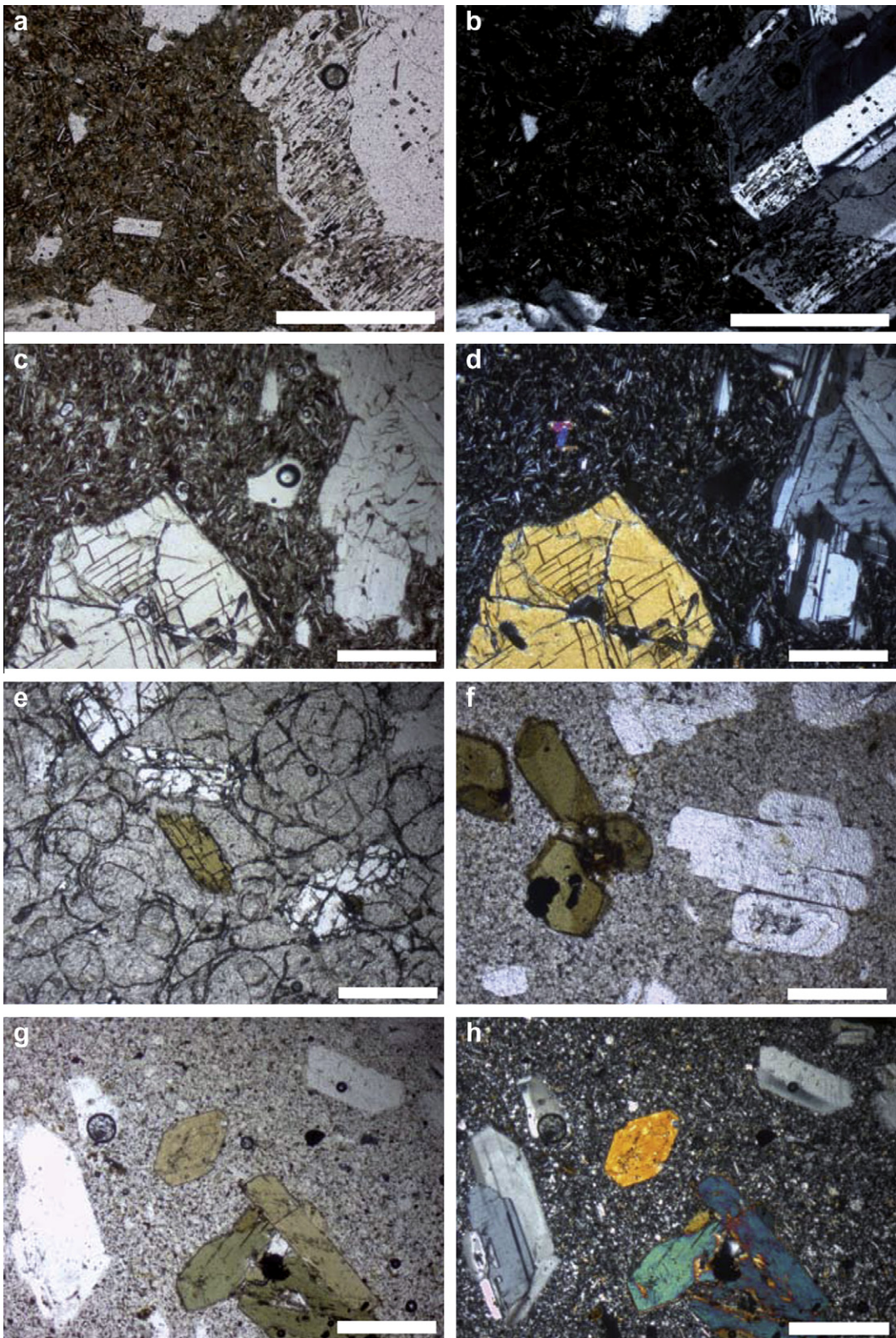


Fig. 6. Photomicrographs of representative lithology types, including geochronology samples. (a and b) Dacite intrusion (A05_117c). (c and d) Basaltic andesite from southwest Ataúro (A05_001). (e) Dacite from the southeast (AT1, A05_054). (f) Dacite (AT3, A05_127). (g and h) Dacite (AT2, A05_107). Scale bar in all images is 0.5 mm long.

All reef limestone overlies the volcanic stratigraphy with no interbedding observed, constraining the maximum age of the oldest, high-level terraces to be younger than the final volcanic activity. Other palaeontological evidence supports construction of the volcanic edifice below the coral growth zone prior to reef development. A small deposit of ferruginous sediment located beneath

the surface of terrace 6 in southeastern Ataúro (8.29943°S , $125.58224^{\circ}\text{E}$, 400 mASL) yielded examples of the deep water dwelling foraminifera *Globorotalia truncatulinoides*.

The youngest sedimentary deposits on the island are alluvial gravels and sands in river valleys and on coastal plains. The extent of these deposits is shown on Fig. 2. Alluvial gravels are mostly

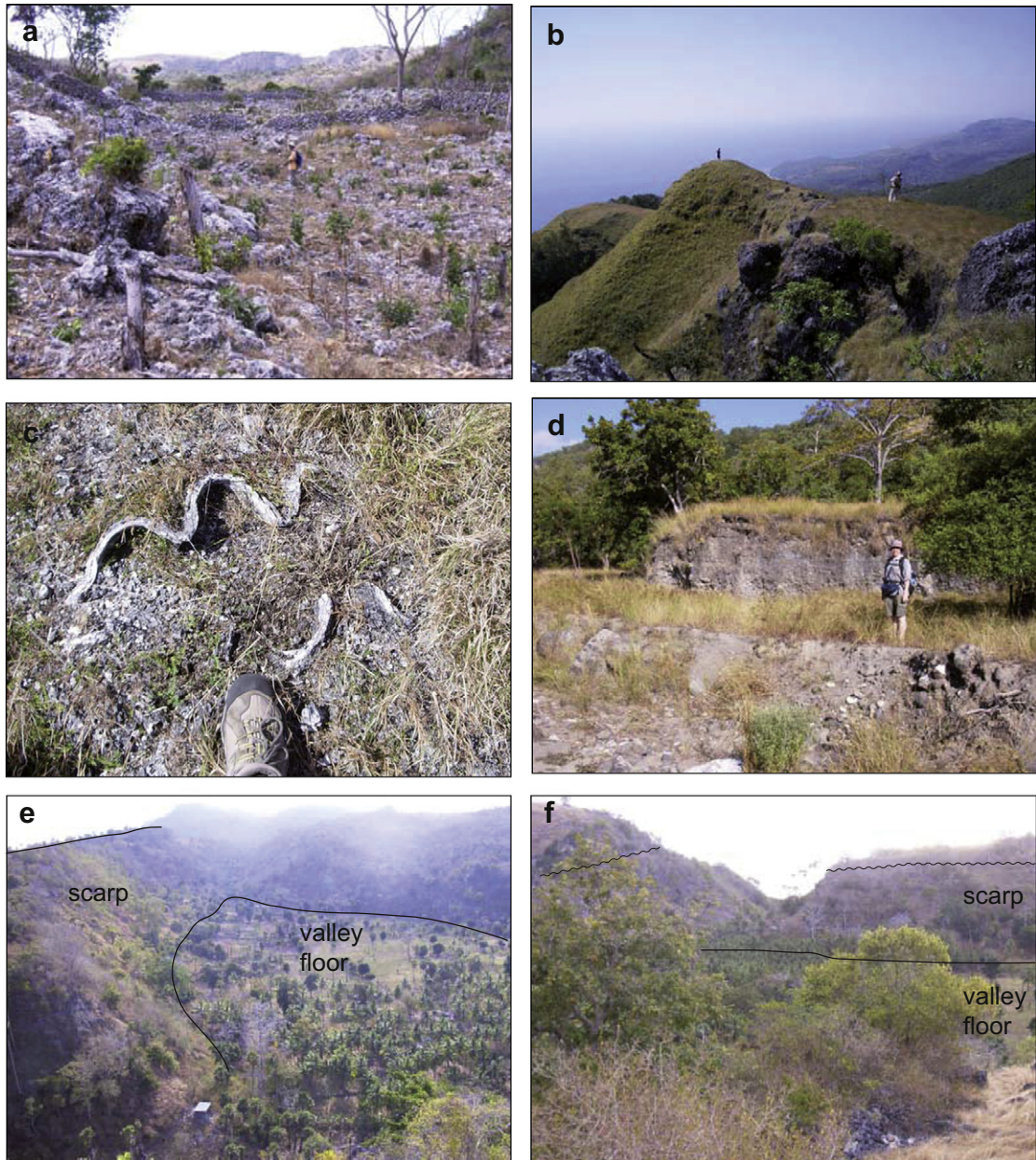


Fig. 7. Terrace and fault related landscape features of Ataúro. (a) Cultivation of thin soils over limestone has resulted in soil loss and bedrock exposure in fields, revealing extensive karstification. This example is near the village of Arlo, northern Ataúro (8.19169° S, 125.58638° E). (b) High terrace levels in southwest Ataúro. (c) Giant clam (*Tridacna* species) fossil on terrace shown in (b) (8.20734° S, 125.57918° E, 570 mASL). (d) Alluvial gravel terraces southwest of Beloi (8.22735° S, 125.59944° E). The creek bed is approximately 40 mASL. (e) Arlo fault scarp, looking north from south of Arlo (8.18663° N, 125.58972° E). Solid line indicates the location of the normal fault. Wavy line shows contact between dacite and overlying limestone. (f) Wind gap in the Arlo scarp, looking west from east of Arlo (8.18728° S, 125.59817° E).

confined to the lowermost reaches of ephemeral streams on the island, where, in some places, terraces have formed at low elevations (Fig. 7d).

2.2.1. Distribution and continuity of uplifted terraces

Chappell and Veeh (1978) documented seven terrace levels on the southern coast near Berau, extending to 320 mASL. New mapping and GPS elevation measurements recorded during this study show the lowermost terraces to be continuous around the southern, western and northern coasts, with each terrace level maintaining constant elevation. Field investigations and satellite image interpretation has enabled the mapping of their terrace levels 1–3 around the island, and established the presence of terraces up to level 6 at the northern end of the island (Fig. 8). The terrace elevations on this northern profile are similar to those on the profile

constructed by Chappell and Veeh (1978) on the south coast at East Nameta. In particular, the northern profile includes their bench levels 1a, 1b, 2 – late and 3a, in addition to all of the primary terrace levels.

The elevation difference between consecutive terrace levels is variable, with the difference increasing at higher terrace elevation. For example, the elevation difference between terraces 1 and 2 is 30 m, increasing to around 80 m between terraces 6 and 7. The presence of reef limestone at significant elevation above terrace 7 implies the presence of much older reef successions.

2.3. Hydrothermal activity

A record of present and past hydrothermal activity is evident in several locations on the east coast of Ataúro, in the hanging wall of

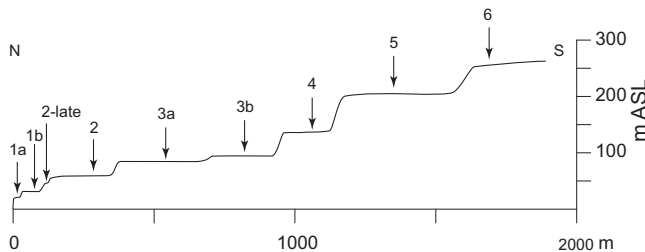


Fig. 8. Topographic profile of terraces extending south from the northernmost point of Ataúro. Designation of terrace levels corresponds with that used by Chappell and Veeh (1978).

the Vila Escarpment. Active hot springs have been recorded at four locations (Fig. 2). The springs are all associated with areas of dacite outcrop, and occur in the intertidal zone. Water temperature at the vents was estimated to be greater than 60 °C. Significant hydrothermal alteration is also evident within the volcanic stratigraphy near Vila and Makili in the southeast of the island. Volcanic textures and primary minerals have been completely destroyed by pervasive hematite–kaolinite alteration in places, and partly replaced in others (Fig. 2). Alteration is also associated with local silicification, disseminated sulphide minerals, including pyrite, and deep weathering. The close proximity of the alteration zone at Makili with a hot spring suggests they both reflect a significant, ongoing hydrothermal system.

2.4. Structure

The Vila Escarpment is the dominant structural expression on Ataúro, and extends along the east flank of Mt. Manucoco, the highest point on the island (Fig. 3c). In detail, the 10 km long Vila Escarpment is the largest of a series of normal faults (Fig. 9), with all other faults located within the hanging wall of the Vila Escarpment. Similarly, the hydrothermal activity described above is also confined to the hanging wall. Faults on Ataúro are typically of north to northeast orientation, and have generated fault scarps of various extents. The central and northern parts of Ataúro feature a series of subparallel, arcuate escarpments up to 5 km long, with a spacing of 100–800 m. Flat bottomed valleys are bounded by the escarpments, which form steep slopes 80–130 m high, and often include cliff sections up to 20 m high at or near the top of the slope (Fig. 7e). The steep escarpments have probable exposures of fault planes in places, although movement indicators are not evident on these planes. Topographic relationships show the majority of faults to have an east-side down sense of movement, suggesting an east to west progression of faults, thus the largest fault, the Vila Escarpment, is the most recent. While signs of active faulting are not readily visible on vegetated slopes, geomorphological evidence suggests that faulting postdates uplift of the island above sea level. A wind gap generated by normal faulting lies immediately to the west of the village of Arlo (Fig. 7f). This village is situated in a 400 m wide valley that is one of several fault-scarp bounded internal drainage basins in the northern part of Ataúro. The limestone terraces are cut by these faults, indicating that uplift above sea level occurred before, or at the same time as, the faults were active.

3. Geochemistry

Major and trace element analyses of 13 samples from Ataúro demonstrate two clear compositional groups; the basaltic andesite of the southwest, and an array of dacite to rhyolite compositions (Figs. 10 and 11). The more felsic rocks exhibit a fractional crystallisation trend, and have a compositional range of 65–71 wt.% SiO₂,

0.7–5 wt.% Fe₂O₃, 0.3–1.4 wt.% MgO, 1–4 wt.% CaO and 2–4 wt.% K₂O (Fig. 12). The basaltic andesite from the southwest part of the island has a distinctly different composition, with much lower SiO₂ (53 wt.%) and K₂O (<1%), and high CaO (13–15 wt.%), Fe₂O₃ (7–8 wt.%) and MgO (8–10 wt.%). Refer to the **Supplementary data for analytical methods and results**.

The rhyolite units of Ataúro are amongst the most felsic rocks in the Banda Arc (Fig. 12), but major and trace element contents show strong similarities with rocks from Wetar and Lirang (Elburg et al., 2005). The basaltic andesites contain much higher levels of Mg, Ca and Cr than other rocks in the Banda Arc, and relatively low amounts of K, Ti, Zr and Sr. The highly porphyritic nature of these rocks, with clinopyroxene and olivine phenocrysts comprising around 50% by mass, suggest that the whole rock analyses are unlikely to be representative of a melt composition. The geochemical variation that occurs within the dacite–rhyolite series of Ataúro, which accounts for 80% of volcanic rocks of the island by area of exposure, fits closely with regional trends, suggesting that Ataúro shares a common volcanic history with adjacent parts of the arc.

4. Geochronology

Discussions regarding the timing of collision in the Banda Arc have placed much emphasis on the timing of cessation of volcanic activity in the Wetar zone (e.g. Elburg et al., 2005; Hirschberger et al., 2005). Given the subsequent uplift of the coral reef terraces that now mantle much of the volcanic edifice to elevations of at least 700 m, it is clear that Ataúro has not been volcanically active for some time. New geochronology, employing the ⁴⁰Ar/³⁹Ar method on hornblende mineral separates, is used here to assess the age of volcanism and provide a constraint on the subduction history within the Wetar zone of the Banda Arc. The establishment of a volcanic stratigraphy of Ataúro now allows geochronology samples to be interpreted in a wider geological context. One of our samples, sample AT1, is interpreted to be the best candidate for representing the youngest parts of the dacitic volcanic stratigraphy. This sample was taken from a structurally intact flank of Mt. Manucoco, west of the Vila Escarpment. Attempts to date the adjacent basaltic andesite sequence were unsuccessful; topographic relationships suggest that these rocks may be contemporaneous or slightly younger than the dacite sequence.

4.1. Previous work

Abbott and Chamalaun (1981) suggested that Ataúro was constructed rapidly from three volcanic centres prior to the cessation of volcanism by 3 Ma. Whole rock K/Ar geochronology yielded average ages of 3.10 ± 0.30 Ma, 3.3 ± 0.8 Ma and 3.46 ± 0.08 Ma for sites in the southeast, southwest and north, respectively (2σ uncertainties quoted; sample locations on Fig. 10). Available geochronology for the southern Banda Arc shows the age of the last recorded magmatism decreases towards the edges of inactive sector of the arc (Fig. 1; Abbott and Chamalaun, 1981; Elburg et al., 2005; Hilton et al., 1992; Honthaas et al., 1998; Scotney et al., 2005). It has been shown that larger islands in the Banda Arc have a more extended volcanic history than Ataúro. Geochronology and tectonic reconstructions suggest that volcanic activity in the Banda Arc commenced ~10 Ma (Hall and Smyth, 2008).

4.2. Methods and results

Hornblende separates were obtained from three hornblende- and plagioclase-phyric dacite samples (AT1–AT3) using standard crushing, heavy liquid and magnetic separation techniques. Samples were then handpicked to obtain clean separates of 90–

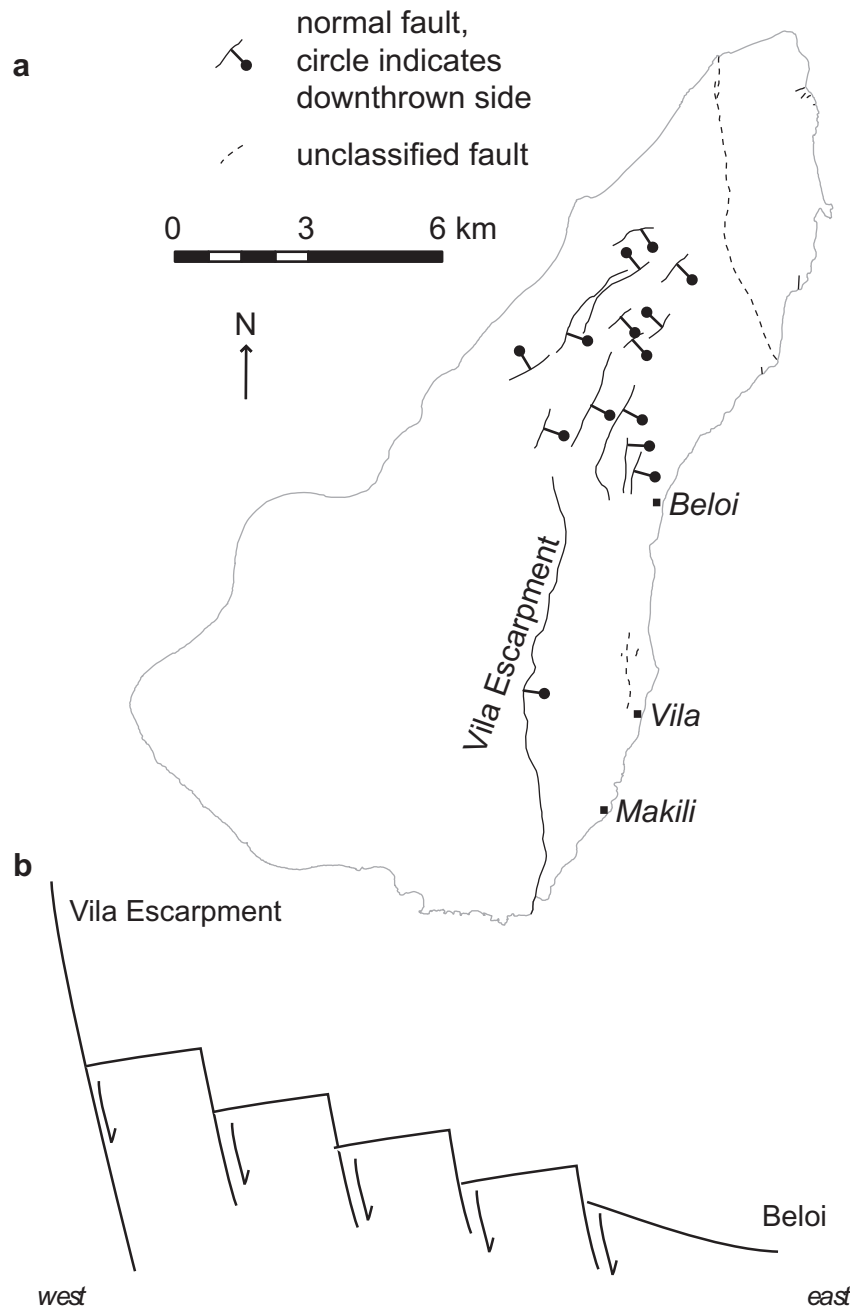


Fig. 9. (a) Summary of faults, from field observations, air photograph and satellite image interpretations. Normal faults east of the Vila Escarpment are dominantly east-side down. (b) Schematic cross section of faulting between the Vila Escarpment and Beloi, on the east coast.

120 mg. Samples were packed in foil, and, together with flux monitors GA1550 biotite (98.8 ± 0.5 Ma (1σ); Renne et al., 1998) and Alder Creek sanidine (1.186 ± 0.0006 Ma; Turrin et al., 1994), were irradiated at the McMaster Nuclear Reactor, Ontario, Canada. $^{40}\text{Ar}/^{39}\text{Ar}$ analyses were conducted at the University of Melbourne Noble Gas Geochronology and Geochemistry Laboratory, using analytical procedures analogous to those described by Phillips et al. (2007). Step-heating analyses of the hornblende separates were carried out using a tantalum furnace connected to a VG3600 mass spectrometer equipped with a Daly detector. Results are presented in Supplementary data Table 3, and the ^{39}Ar release spectra, plotted using Isoplot/Ex3.04 (Ludwig, 2003) shown in Fig. 13. Two aliquots of each sample were analysed. All results are reported with 2σ uncertainty.

Sample AT1a yielded a plateau age of 3.27 ± 0.18 Ma, defined by six contiguous steps containing 86% of the ^{39}Ar released. This plateau age is taken to be a reliable estimate of the time of eruption. The second aliquot, AT1b, produced a saddle-shaped spectrum with a minimum age of 3.65 ± 0.18 Ma indicated by a single step accounting for 42% of the ^{39}Ar released. The saddle-shaped spectrum is attributed to contamination by excess argon, therefore this age only represents a maximum age for the time of eruption.

Sample AT2a did not produce a statistically valid plateau, although four contiguous steps, comprising 81% of the ^{39}Ar released, have similar apparent ages, with a weighted mean age of 4.67 ± 0.37 Ma. Sample AT2b yielded an apparent age of 4.32 ± 0.27 Ma, comprising 76% of the ^{39}Ar released in a single temperature step. Both aliquots produced saddle-shaped spectra,

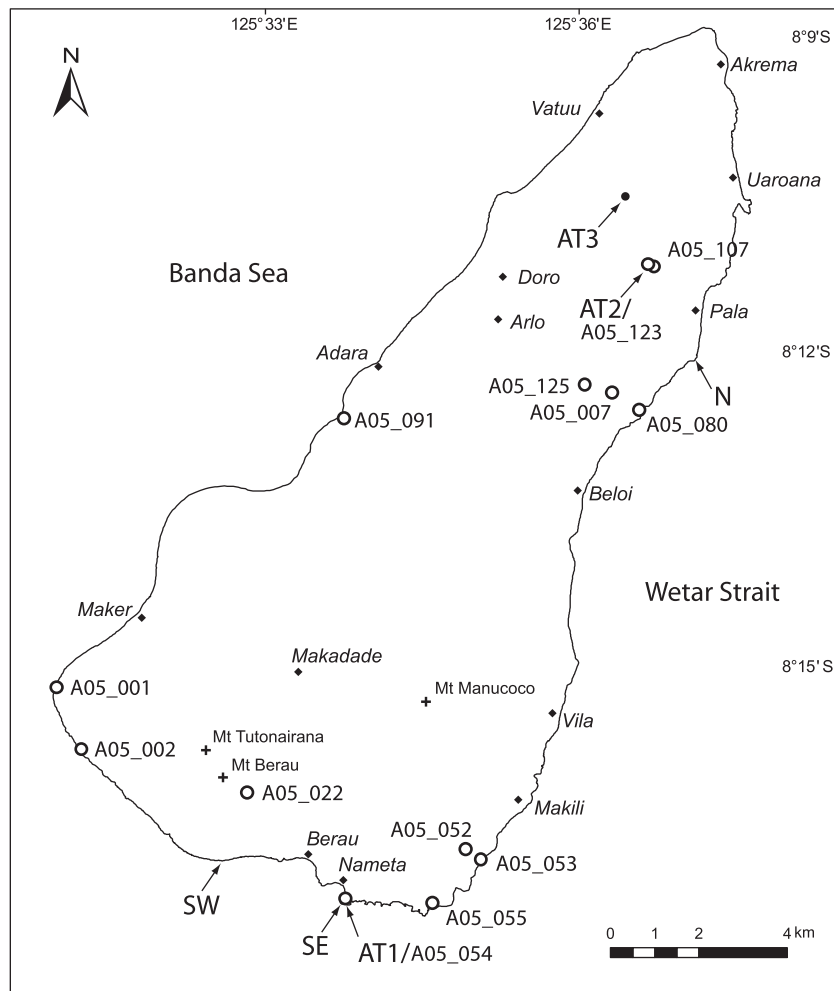


Fig. 10. The locations of geochemistry samples are denoted by open circles, and geochronology sample sites (AT1–AT3, this study) are indicated by arrows. Locations labelled SW, SE and N are those of Abbott and Chamalaun (1981). Coordinates of geochronology sample sites are as follows: AT1, 8.30549°S, 125.56152°E; AT2, 8.17578°S, 125.62414°E; AT4, 8.26242°S, 125.50154°E. Refer to the Supplementary data for locations of geochemistry samples.

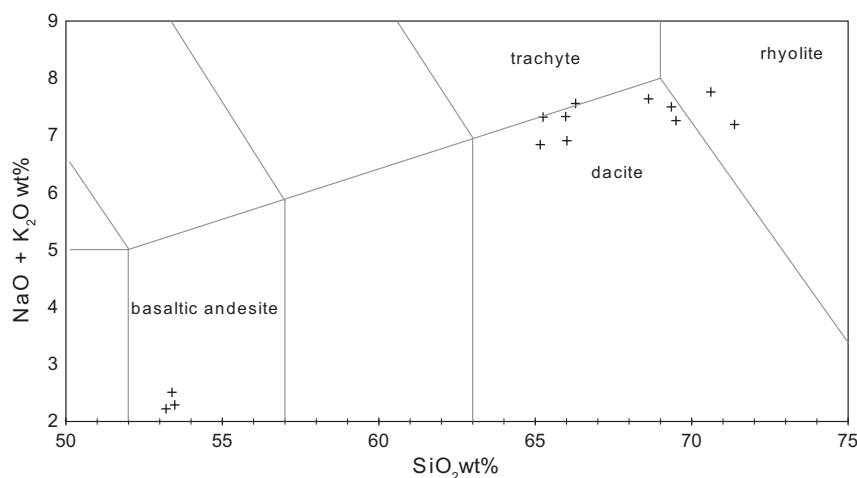


Fig. 11. Total alkalis plot of Ataúro whole rock geochemical analyses. The majority of samples form a trend from dacite to rhyolite compositions.

suggesting the presence of excess argon, therefore these ages represent maximum estimates for the time of eruption. Low Ca/K in the low temperature steps may be the result of outgassing of fluid inclusions or a relatively calcium-poor mineral contaminant.

The broadly saddle-shaped spectra of sample AT3a is disturbed by an anomalous step with an apparent age around 10 Ma. The age indicated by the youngest step, 3.13 ± 0.19 Ma, is within error of the plateau age of sample AT1a. Sample AT3b produced a strongly

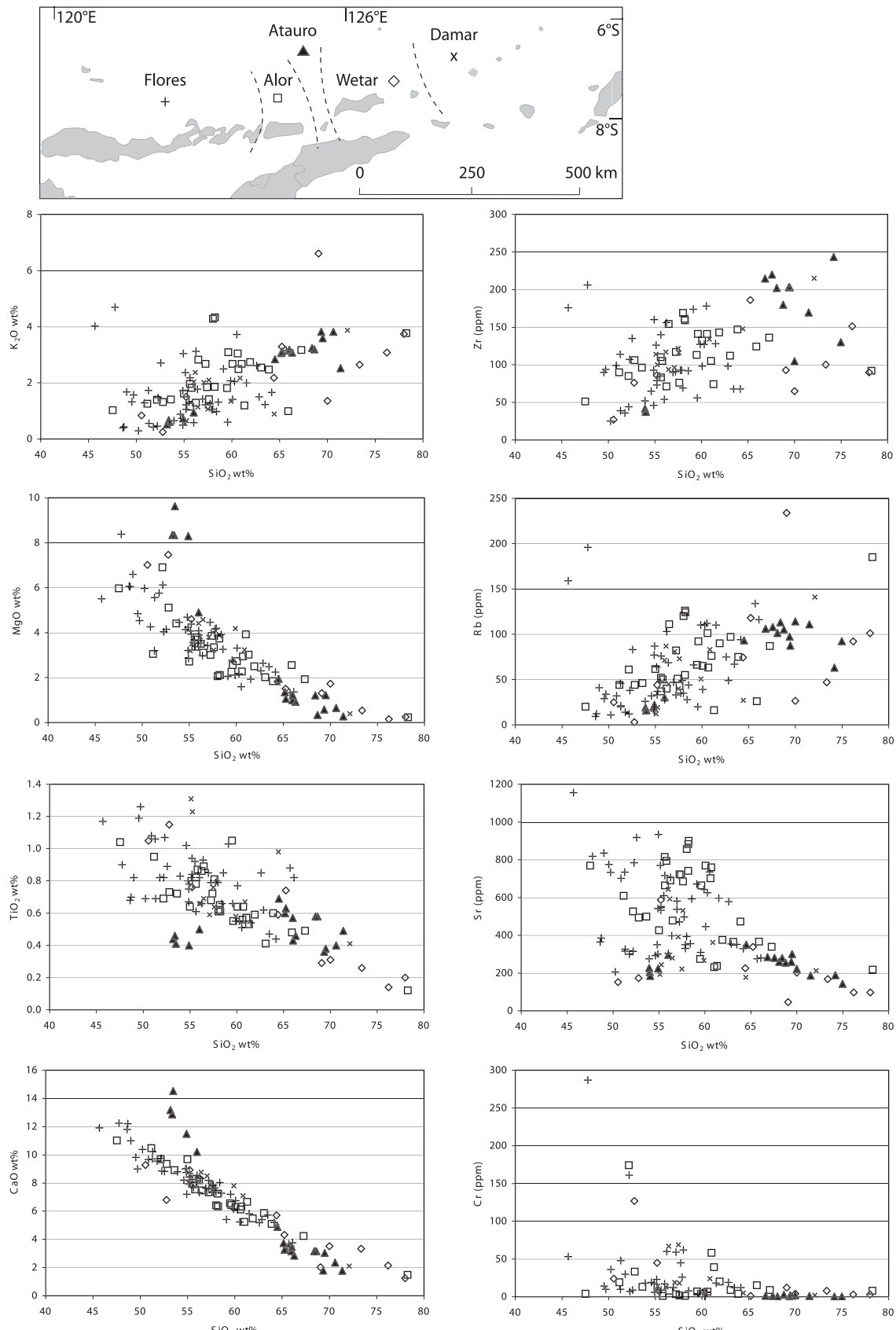


Fig. 12. Harker variation diagrams of selected major and trace elements, illustrating along arc compositional variation. As illustrated on the location map, analyses are divided into the following segments: Ataúro (solid triangles), Wetar (includes Wetar, Lirang and Romang, open diamonds), Alor (includes Alor and islands in the Pantar Strait, open squares), Flores (Pantar, west to Flores, +) and Damar (Damar and farther east, x). High Cr (550–900 ppm) samples from Ataúro are excluded from the Cr vs SiO_2 plot for clarity. Data from Elburg et al. (2005, 2002), Honthaas et al. (1998), Stolz et al. (1990), van Bergen et al. (1989), Wheller et al. (1987) and Whitford et al. (1977).

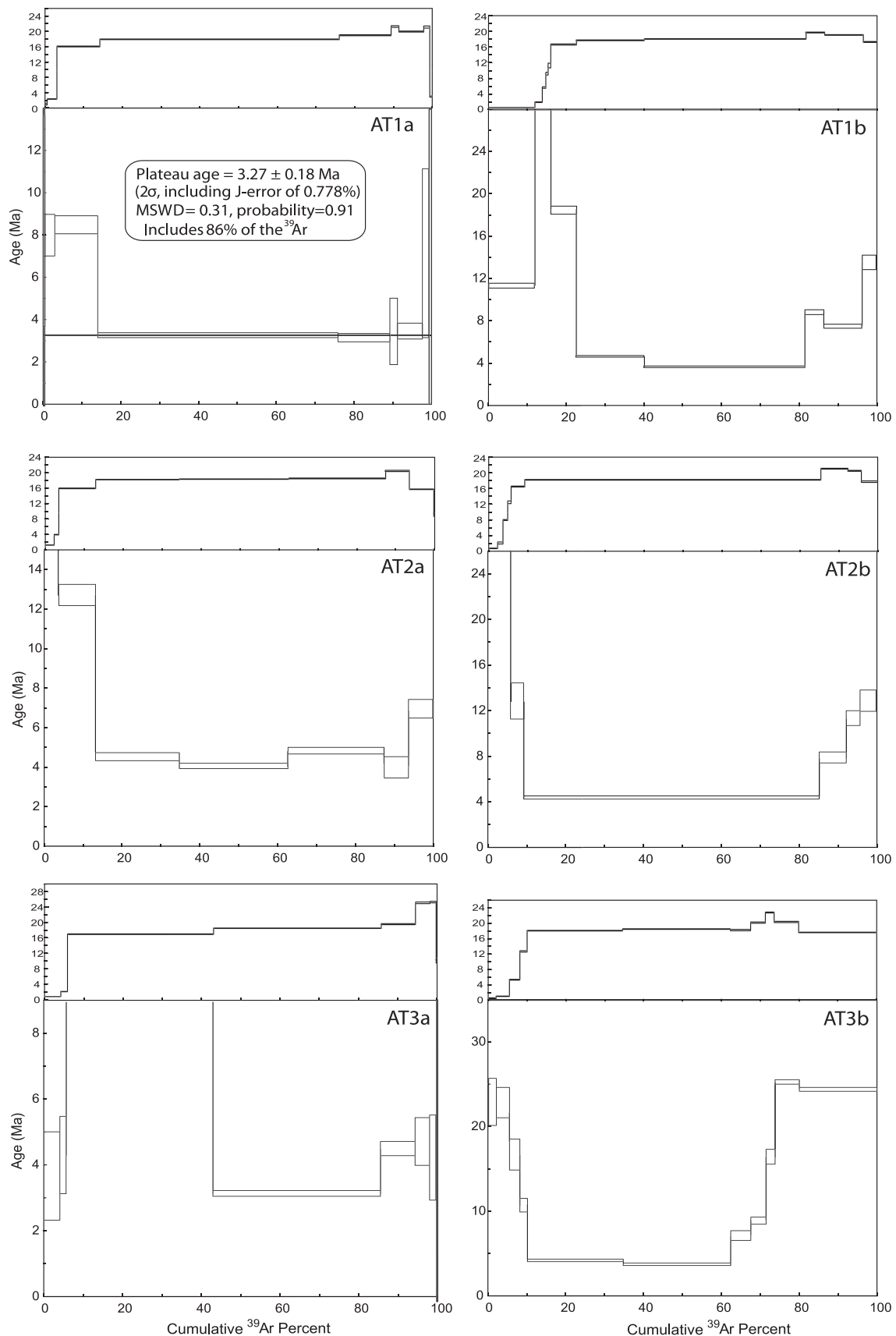


Fig. 13. $^{40}\text{Ar}/^{39}\text{Ar}$ and Ca/K step-heating spectra for hornblende samples AT1, AT2 and AT3. Box heights are $\pm 1\sigma$.

saddle-shaped spectrum, with high apparent ages at both low and high temperature steps. The youngest apparent age was produced by two contiguous steps in the centre of the spectrum with a weighted mean age of 3.85 ± 0.30 Ma, which account for 52% of the ^{39}Ar released.

The plateau age of 3.27 ± 0.18 Ma reported here for sample AT1a, from southeastern Ataúro, is consistent with volcanism having ceased by 3 Ma. This result is similar to, but slightly more precise than, the K/Ar data from the same area (Abbott and Chamalaun, 1981).

5. Seismicity in the wetar zone

Earthquake datasets provide insight into active deformation of the lithosphere and deeper subduction zone processes. Previous work investigating the nature of earthquakes in the Banda Arc includes both regional (Das, 2004; McCaffrey, 1988; Schoffel and Das, 1999) and more focussed studies (Ely and Sandiford, 2010; McCaffrey et al., 1985; Sandiford, 2008). Compared to other parts of the Banda Arc, seismicity in the Wetar zone has unique characteristics that have important implications for understanding the development of the collision zone. The earthquake catalogue of the Global CMT Project (2008) shows that shallow (<70 km depth) seismicity in the Wetar zone is largely restricted to north of the volcanic arc, where reverse fault mechanism earthquakes are associated with the Wetar Thrust (Fig. 14a) and seem to account for most of the convergence in the Timor region resulting from the northeast motion of the Australian plate. Notable events south of the volcanic arc include two large magnitude (>6) normal fault mechanism events with an orientation consistent with arc-parallel extension. This change in orientation of earthquake events across the arc implies significant partitioning of deformation across the arc.

A defining feature of the Wetar zone is the absence of intermediate depth seismicity, extending from 70 km to 350 km below surface (Fig. 14b). This aseismic zone, known as the Wetar seismic gap (Ely and Sandiford, 2010), is unique within the Sunda-Banda arc as, at these depths, seismicity is recorded in all other regions of the Banda Arc, and particularly immediately east of the Wetar zone (Sandiford, 2008) (Fig. 14d). Zones of low or absent seismicity in the Sunda-Banda subduction zone are common at depths of >350 km, where they may be explained by a transition in the nature of stress and heterogeneity within the slab (Das, 2004). In contrast, due to the shallow depth, the complete absence of seismicity, and lack of active volcanism, the Wetar seismic gap is interpreted to be a result of breakoff of the subducting slab from the surface plate during the collision process.

Assuming that plate velocities and subduction rates have remained relatively constant during Plio-Pleistocene times, the depth of the base of the Wetar seismic gap constrains the amount of subduction since the onset of slab rupture. At a rate of around 70 km/m.y. (Bock et al., 2003; Genrich et al., 1996; Nugroho et al., 2009), the vertical extent of the seismic gap (280 km) suggests that slab rupture occurred at 4 Ma. Below 350 km, seismicity in the Wetar zone shows similar trends to more typical subduction zones in terms of distribution and orientation of earthquake events.

6. Discussion

6.1. Geological history

Ataúro comprises a subaqueous volcanic sequence intruded by dykes and sills up to several hundred metres in length. The perlitic texture observed in many samples is common in lavas erupted in an aqueous environment, and is a result of hydration and

expansion of glass (McBirney, 2007). The presence of extensive sedimentary deposits with features such as cross bedding is also consistent with subaqueous eruption and deposition of volcanic products. Unlike the neighbouring islands of Wetar and Alor, interbedded volcanic and limestone sequences have not been found, suggesting that the volcanic edifice formed below the coral growth zone, or alternatively, at a rate too rapid to allow reef formation. Further supporting evidence for a relatively deep water environment following eruption is provided by the presence of the planktonic foraminifera *Globorotalia truncatulinoides* in a ferruginous deposit now at an elevation of 400 mASL. This benthic species mostly occurs at depths greater than 200 m (Mulitza et al., 1997; Ravelo and Fairbanks, 1992).

The distribution of the two geochemically distinct volcanic sequences on Ataúro suggests that the volcanic succession built up from at least two volcanic centres. In the southwest of the island, the distinctive basaltic andesite composition and lava flow directions imply Mt. Tutonairana and Mt. Berau mark the location of a volcanic eruption centre, as initially suggested by Abbott and Chamalaun (1981). The location of other volcanic centres responsible for the great volume of dacitic material that forms the eastern and northern parts of the island requires further consideration. Based on normal volcanic morphology, the highest point of the island is a possible candidate to be a volcanic centre, and has been suggested as such (Abbott and Chamalaun, 1981). Yet, other evidence indicates that this is not the case. There is no progression from distal to proximal volcanic facies associated with this topographic high that would be expected if it were a volcanic centre. Also, there is no evidence of volcanic landform features preserved. Rather, the footwall of the Vila Escarpment forms the eastern flank of this high ridge. The southwest dip of volcaniclastic sediments in all parts of eastern Ataúro suggests a volcanic eruption centre was located to the northeast of the island. Coarse-grained intrusive rocks such as granodiorite, found at deep erosion levels on Wetar, Lirang and Alor, do not occur on Ataúro, reflecting a higher erosion level in the magmatic system or a less complex magmatic history than the larger islands (Abbott and Chamalaun, 1981; Elburg et al., 2005).

Flights of coral reef limestone terraces preserve a record of uplift following the cessation of magmatism. Seven distinct terrace levels have been recognised, and the presence of limestone at higher elevations, up to 700 mASL, implies that additional reef terraces may be present. The continuity of terraces around the southern, western and northern sides of the island at constant elevation demonstrates most of the island has been subject to uniform uplift. The exception to this occurs with the faulted terrain between the Vila Escarpment and the east coast, especially near Beloi and Arlo, where distinct tilted fault blocks offset terraces. Uplift on a regional scale along the volcanic arc is demonstrated by the presence of coral terrace flights on adjacent islands, including Alor and Wetar (Chappell and Veeh, 1978; Hantoro et al., 1994; van Bemmelen, 1949).

6.2. Deformation processes

Ataúro preserves evidence of two distinct modes of deformation: uplift and east–west extension, distinguished by the way they deform terrace sequences. Normal fault affected terraces along the east coast of Ataúro form rotated tilt blocks, back-tilted to the west along steep east-dipping fault planes. In contrast, elsewhere on the island uplifted, horizontal terrace sequences imply a regional uplift with no tilting. In order to understand the timing, mechanisms involved, and the scale over which they occur, the nature of deformation throughout the Wetar zone is considered here. While the lack of detailed geological maps available for Alor and Wetar makes direct comparison between islands difficult, the earthquake record

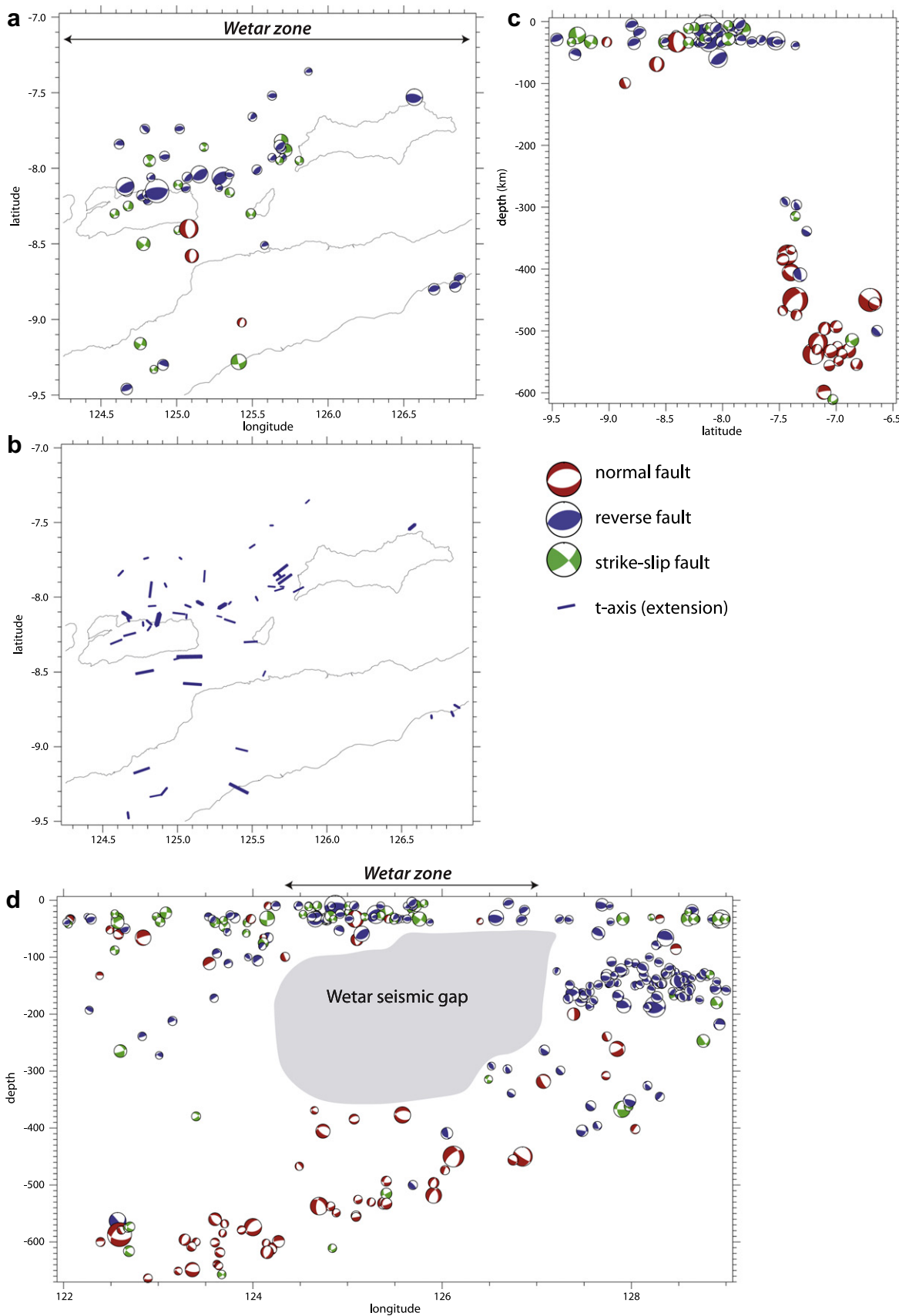


Fig. 14. CMT catalogue seismicity in the Wetar zone. (a) Map of shallow (<70 km depth) events ($n = 51$). (b) Map of shallow events showing orientation of t -axes (orientation of extension). (c) Cross section of all events ($n = 288$) in the Wetar zone showing vertical extent of the Wetar seismic gap (WSG). (d) Projected long section showing the along strike extent of the WSG (grey shading), bounded in the east by a zone of intense seismicity interpreted to be the result of an eastern propagating tear of the slab (Sandiford, 2008).

and seismic reflection profiles offer an insight into the nature of regional scale deformation in the Wetar zone. In particular, the distribution of shallow earthquakes shows active deformation to be strongly partitioned, and the majority of earthquakes can be attributed to north–south directed compression on the Wetar thrust. Focal mechanism solutions for the few earthquakes recorded south of the thrust zone show movement on normal and left lateral strike-slip faults consistent with east–west extension parallel to the Wetar Strait. Cross cutting relationships between uplifted terraces and normal faults on Ataúro suggest late onset of extension relative to uplift.

At sublithospheric depths the Wetar zone is remarkable for a lack of earthquakes. This region, the Wetar seismic gap, underlies Alor, Ataúro and Wetar and extends to a depth of 350 km. The seismic gap is thought to represent a zone of slab rupture that is currently propagating most rapidly to the east, beneath Romang. Wortel and Spakman (2000) presented a model that showed how this type of slab rupture results in subsidence at the point of tear propagation, and uplift in the zone over where the down-going slab has detached from the surface plate. Surface movement can be seen as a result of the partitioning of the slab pull force. Uplift occurs as a result of a reduction in slab pull as the slab is detached, then transfer of this stress to the point of tear results in an increased slab pull, leading to subsidence. This pattern of topographic expression is seen in the Banda Arc. There is evidence of uplift throughout the Wetar zone. Farther east, beyond the point of slab rupture (Sandiford, 2008), the Banda Arc has a subdued topographic expression of low volcanic islands separated by deep sea passages.

The uniform nature of uplift of Ataúro and throughout the Wetar zone, and the early onset of such uplift relative to normal faulting, is difficult to reconcile in the context of the uplift being fault related displacement. It would be expected that uplift as a result of movement on east–west oriented thrust faults would generate tilted blocks and a more irregular uplift pattern than is evident. The occurrence of terraces of constant elevation extending around the southern, western and northern coastlines is not consistent with thrust related uplift, and is more readily attributed to the process of slab detachment as described above.

East of the Vila Escarpment, brittle faulting has tilted terrace surfaces, forming blocks on the order of several hundreds of metres. Faults cross-cut limestone terraces, therefore movement on these faults was contemporaneous with, or postdated, uplift of the coral reefs above sea level. Preservation of landscape features such as wind gaps suggests that the normal faults are relatively young structures, and that they may still be active. These tilted terrace surfaces, and the associated fault scarps, are part of a complex of north–northeast oriented normal faults, mostly with an east-side down sense of movement (Fig. 9). This structural trend is evident throughout the Wetar zone. Breen et al. (1989) concluded that left lateral offset of the arc has occurred along the Wetar–Ataúro Fault between Ataúro and Liran. While the fault set of Ataúro described in this paper has the same trend as this structure, no evidence for strike-slip movement was recorded. Fault sets also with north–northeast orientations, but unknown sense of movement, have also been noted on Alor (Silver et al., 1983) and Wetar (Scotney et al., 2005).

As discussed in Section 6.1, stratigraphic evidence supports the presence of an eruption centre located to the northeast of the island, and while available bathymetry is of too low resolution to confirm the presence of an offshore collapsed volcanic edifice, the pattern of normal faults with down-throw to the east is consistent with collapse of such a feature. The occurrence of earthquakes with similar focal mechanism solutions to those recorded south of Alor (east–west extension) may have triggered such a collapse. The suggestion that these normal faults are evidence of collapse of a

volcanic centre implies that Ataúro must have formerly been a larger, and topographically higher, island.

6.3. Implications for timing of arc–continent collision

The new $^{40}\text{Ar}/^{39}\text{Ar}$ age data presented here data shows that there was active volcanism on Ataúro until at least 3.3 Ma, with the implication that subduction remained active until this time. The cessation of volcanism has been linked to the onset of collision (Abbott and Chamalaun, 1981; Elburg et al., 2005; Hall, 1996), yet the timing relationship between the end of volcanism and collision is not straightforward. One variable that must be considered is the depth of magma generation. Magma production in subduction zones occurs at depths of 65–130 km (England et al., 2004). If a simple model is considered where collision results in rupture of the subducting oceanic lithosphere from the continental margin at or near the surface, at the current rate of movement of the Indo-Australian plate (~ 7 cm/year) this would result in the edge of the oceanic plate passing through the magma generation zone as much as 1–2 million years after rupture. Alternatively, depending on the buoyancy, strength and velocity of the slab, part of the continental lithosphere may be subducted, prior to slab breakoff occurring at greater depths (De Franco et al., 2008). This scenario would result in a shorter delay between locking of the subduction zone by continental lithosphere unable to subduct and last magma production. The absence of a seismically active slab above depths of 350 km is consistent with slab breakoff commencing at 4 Ma, and, in conjunction with the continuation of volcanism until 3.3 Ma, implies a maximum age for the termination of subduction of Australian lithosphere along the Wetar zone segment of the Banda arc.

Acknowledgements

Field work on Ataúro was made possible with the assistance of the National Directorate for Geology and Minerals, Timor-Leste. Thanks to Katherine Harper and Daniel Ervin for their contributions to the field mapping project. Detailed reviews by Tim Charlton and Ron Harris were very helpful in sharpening the focus of the manuscript. KE acknowledges the support of a CSIRO Postgraduate Award and the David Hay Postgraduate Writing-Up Award.

Appendix A. Supplementary material

Supplementary data associated with this article can be found, in the online version, at doi:10.1016/j.jseas.2011.01.019.

References

- Abbott, M.J., Chamalaun, F.H., 1981. Geochronology of some Banda Arc volcanics. In: Wirojyono, S. (Ed.), *The Geology and Tectonics of Eastern Indonesia*. Geological Research and Development Centre, Spec. Pub. 2, pp. 253–271.
- Bock, Y., Prawirodiridjo, L., Genrich, J.F., Stevens, C.W., McCaffrey, R., Subarya, C., Puntodewo, S.S.O., Calais, E., 2003. Crustal motion in Indonesia from global positioning system measurements. *Journal of Geophysical Research* 108 (B8), 2367. doi:10.1029/2001JB000324.
- Breen, N.A., Silver, E.A., Roof, S., 1989. The Wetar back arc thrust belt, eastern Indonesia: the effect of accretion against an irregularly shaped arc. *Tectonics* 8 (1), 85–98.
- Chappell, J., Veeh, H.H., 1978. Late Quaternary tectonic movements and sea-level changes at Timor and Atauro Island. *Geological Society of America Bulletin* 89 (3), 356–368.
- Das, S., 2004. Seismicity gaps and the shape of the seismic zone in the Banda Sea region from relocated hypocenters. *Journal of Geophysical Research* 109 (B12), B12303.
- De Franco, R., Govers, R., Wortel, R., 2008. Dynamics of continental collision: influence of the plate contact. *Geophysical Journal International* 174 (3), 1101–1120.
- Elburg, M.A., van Bergen, M., Hoogewerff, J., Foden, J., Vroon, P., Zulkarnain, I., Nasution, A., 2002. Geochemical trends across an arc–continent collision zone: magma sources and slab-wedge transfer processes below the Panter Strait volcanoes, Indonesia. *Geochimica et Cosmochimica Acta* 66 (15), 2771–2789.

- Elburg, M.A., Foden, J.D., van Bergen, M.J., Zulkarnain, I., 2005. Australia and Indonesia in collision: geochemical sources of magmatism. *Journal of Volcanology and Geothermal Research* 140 (1–3), 25–47.
- Ely, K.S., Sandiford, M., 2010. Seismic response to slab rupture and variation in lithospheric structure beneath the Savu Sea, Indonesia. *Tectonophysics* 438 (1–2), 112–124. doi:10.1016/j.tecto.2009.08.027.
- England, P., Engdahl, R., Thatcher, W., 2004. Systematic variation in the depths of slabs beneath arc volcanoes. *Geophysical Journal International* 156 (2), 377–408.
- Genrich, J.F., Beck, Y., McCaffrey, R., Calais, E., Stevens, C.W., Subarya, C., 1996. Accretion of the southern Banda arc to the Australian plate margin determined by Global Positioning System measurements. *Tectonics* 15 (2), 288–295.
- Hall, R., 1996. Reconstructing Cenozoic SE Asia. In: Hall, R., Blundell, D.J. (Eds.), *Tectonic Evolution of Southeast Asia*. Geological Society of London Special Publication 106, pp. 153–184.
- Hall, R., Smyth, H.R., 2008. Cenozoic arc processes in Indonesia: identification of the key influences on the stratigraphic record in active volcanic arcs. In: Draut, A.E., Clift, P.D., Scholl, D.W. (Eds.), *Formation and Applications of the Sedimentary Record in Arc Collision Zones: The Geological Society of America Special Paper* 436, pp. 27–54.
- Hall, R., Wilson, M.E.J., 2000. Neogene sutures in eastern Indonesia. *Journal of Asian Earth Sciences* 18 (6), 781–808.
- Hantoro, W.S., Pirazzoli, P.A., Jouannic, C., Faure, H., Hoang, C.T., Radtke, U., Causse, C., Borel Best, M., Lafont, R., Bieda, S., Lambeck, K., 1994. Quaternary uplifted coral reef terraces on Alor Island, East Indonesia. *Coral Reefs* 13 (4), 215–223.
- Hilton, D.R., Hoogewerff, J.A., van Bergen, M.J., Hammerschmidt, K., 1992. Mapping magma sources in the east Sunda-Banda arcs, Indonesia: constraints from helium isotopes. *Geochimica et Cosmochimica Acta* 56 (2), 851–859.
- Hinschberger, F., Malod, J.A., Rehault, J.P., Villeneuve, M., Royer, J.Y., Burhanuddin, S., 2005. Late Cenozoic geodynamic evolution of eastern Indonesia. *Tectonophysics* 404 (1–2), 91–118.
- Honthaas, C., Rehault, J.P., Maury, R.C., Bellon, H., Hemond, C., Malod, J.A., Cornee, J.J., Villeneuve, M., Cotten, J., Burhanuddin, S., Guillou, H., Arnaud, N., 1998. A Neogene back-arc origin for the Banda Sea basins: geochemical and geochronological constraints from the Banda ridges (East Indonesia). *Tectonophysics* 298 (4), 297–317.
- Ludwig, K.R., 2003. Isoplot 3.00 A Geochronological Toolkit for Microsoft Excel. Berkeley Geochronology Center Special Publication No. 4.
- McBirney, A.R., 2007. Igneous Petrology. Jones and Bartlett, Boston, 550pp.
- McCaffrey, R., 1988. Active tectonics of the eastern Sunda and Banda arcs. *Journal of Geophysical Research* 93 (B12), 15163–15182.
- McCaffrey, R., Molnar, P., Roecker, S.W., Joyodiwiryo, Y.S., 1985. Microearthquake seismicity and fault plane solutions related to arc-continent collision in the eastern Sunda Arc, Indonesia. *Journal of Geophysical Research* 90 (B6), 4511–4528.
- Mulitza, S., Durkoop, A., Hale, W., Wefer, G., Niebler, H.S., 1997. Planktonic foraminifera as recorders of past surface-water stratification. *Geology* 25 (4), 335–338.
- Nugroho, H., Harris, R., Lestariya, A.W., Maruf, B., 2009. Plate boundary reorganization in the active Banda Arc-continent collision: Insights from new GPS measurements. *Tectonics* 29, 52–65. doi:10.1016/j.tecto.2009.01.026.
- Phillips, G., Wilson, C.J.L., Phillips, D., Szczepanski, S., 2007. Thermochronological ($^{40}\text{Ar}/^{39}\text{Ar}$) evidence for Early Palaeozoic basin inversion within the southern Prince Charles Mountains, East Antarctica: Implications for East Gondwana. *Journal of the Geological Society* 164, 771–784.
- Ravelo, A.C., Fairbanks, R.G., 1992. Oxygen Isotopic Composition of Multiple Species of Planktonic Foraminifera: Recorders of the Modern Photic Zone Temperature Gradient. *Paleoceanography* 7 (6), 815–831.
- Renne, P.R., Swisher, C.C., Deino, A.L., Karner, D.B., Owens, T.L., DePaolo, D.J., 1998. Intercalibration of standards, absolute ages and uncertainties in $^{40}\text{Ar}/^{39}\text{Ar}$ dating. *Chemical Geology* 145, 117–152.
- Sandiford, M., 2008. Seismic moment release during slab rupture beneath the Banda Sea. *Geophysical Journal International* 174 (2), 659–671.
- Schoffel, H.J., Das, S., 1999. Fine details of the Wadati-Benioff zone under Indonesia and its geodynamic implications. *Journal of Geophysical Research* 104 (B6), 13101–13114.
- Scotney, P.M., Roberts, S., Herrington, R.J., Boyce, A.J., Burgess, R., 2005. The development of volcanic hosted massive sulfide and barite-gold orebodies on Wetar Island, Indonesia. *Mineralium Deposita* 40 (1), 76–99.
- Silver, E.A., Reed, D., McCaffrey, R., Joyodiwiryo, Y., 1983. Back arc thrusting in the eastern Sunda Arc, Indonesia: a consequence of arc-continent collision. *Journal of Geophysical Research* 88 (B9), 7429–7448.
- Stolz, A.J., Varne, R., Davies, G.R., Wheller, G.E., Foden, J.D., 1990. Magma source components in an arc-continent collision zone: the Flores-Lembata sector, Sunda arc, Indonesia. *Contributions to Mineralogy and Petrology* 105 (5), 585–601.
- The Global CMT Project, 2008. <<http://www.globalcmt.org>>.
- Turpin, B.D., Donnelly-Nolan, J.M., Hearn, B.C., 1994. $^{40}\text{Ar}/^{39}\text{Ar}$ ages from the rhyolite of Alder Creek, California – age of the Cobb Mountain normal polarity subchron revisited. *Geology* 22 (3), 251–254.
- van Bemmelen, R.W., 1949. The Geology of Indonesia, vol. IA. General Geology of Indonesia and Adjacent Archipelagoes. Government Printing Office, The Hague, 732pp.
- van Bergen, M.J., Erfan, R.D., Sriwana, T., Suharyono, K., Poorter, R.P.E., Varekamp, J.C., Vroon, P.Z., Wirakusumah, A.D., 1989. Spatial geochemical variations of arc volcanism around the Banda Sea, Netherlands. *Journal of Sea Research* 24 (2–3), 313.
- Wheller, G.E., Varne, R., Foden, J.D., Abbott, M.J., 1987. Geochemistry of Quaternary volcanism in the Sunda-Banda Arc, Indonesia, and 3-component genesis of island-arc basaltic magmas. *Journal of Volcanology and Geothermal Research* 32 (1–3), 137–160.
- Whitford, D.J., Compston, W., Nicholls, I.A., Abbott, M.J., 1977. Geochemistry of late Cenozoic lavas from eastern Indonesia: role of subducted sediments in petrogenesis. *Geology* 5 (9), 571–575.
- Wortel, M.J.R., Spakman, W., 2000. Subduction and slab detachment in the Mediterranean-Carpathian region. *Science* 290, 1910–1917.